FOS SPECTROSCOPY OF RESOLVED STRUCTURE IN THE NUCLEUS OF NGC 1068

S. CAGANOFF,[1] R. R. J. ANTONUCCI,[2] H. C. FORD,[1,3] G. A. KRISS,[1] G. HARTIG,[3] L. ARMUS,[1] I. N. EVANS,[3]
E. ROSENBLATT,[4] R. C. BOHLIN,[3] AND A. L. KINNEY[3]

ABSTRACT

We report the results of FOS spectroscopy of the continuum peak of NGC 1068 in the wavelength range 2200–7000 Å. Detailed analysis reveals the emission lines to be complex in shape and to consist of a number of different velocity components. Both the Balmer lines and the strong forbidden lines have a contribution from a component with full width at half-maximum on the order of 2200 km s^{-1}. However, we do not detect the broad Hβ emission observed in polarized light. This implies that the continuum peak is not the mirror which reflects light from the hidden Seyfert 1 nucleus. It could possibly contribute some of the reflected light, but the equivalent width of the Hβ BLR line, if present at all, is much weaker than expected from the ground-based nuclear polarized-flux spectrum.

Subject headings: galaxies: individual (NGC 1068) — galaxies: nuclei — galaxies: Seyfert — ultraviolet: spectra

1. INTRODUCTION

Many of our current insights regarding the nature of Seyfert galaxies have stemmed from studies of NGC 1068, the nearest and most luminous known example of the Seyfert 2 class of active spirals (see Osterbrock 1989 for an excellent review). A particularly interesting discovery was made by Antonucci & Miller (1985) who found that NGC 1068 exhibits a Seyfert 1 spectrum with broad permitted lines when viewed in polarized light. This phenomenon is interpreted as light from a hidden Seyfert 1 nucleus being reflected by electron scattering into the observer's line of sight by a hot plasma or "mirror" (Miller, Goodrich, & Mathews 1991, hereafter MGM). In unpolarized light, broad lines reflected from the hidden Seyfert 1 nucleus are dominated by emission from the directly observed narrow line region and the host galaxy starlight, whereas observation in polarized light emphasizes the reflected emission, yielding a Seyfert 1 spectrum. This observation constitutes strong evidence for the hypothesis that Seyfert 1 and Seyfert 2 nuclei are intrinsically the same type of object but "appear" different because of viewing angle.

In Paper I, Evans et al. (1991) presented the first high-resolution narrow-band view of NGC 1068, provided by the *Hubble Space Telescope* Planetary Camera (*HST* PC). The narrow band image in the light of [O III] λ5007 reveals a "cone" of emission consistent in position angle and opening angle with the ionization cone observed by Pogge (1988). This cone is attributed to anisotropic ionizing radiation from the hidden Seyfert 1 nucleus. The apex of the cone lies south of emission-line cloud B (see Paper I). The PC continuum image presented by Lynds et al. (1991) exhibits a strong, partially resolved peak located just north of cloud B (Paper I). The continuum peak is not coincident with the apex of the emission-line cone, suggesting that the continuum peak is *not*

the active nucleus of NGC 1068 (see Paper I and also Planesas, Scoville, & Myers 1991 for other evidence that the cone apex is actually the true nucleus). The continuum peak may be reflected light from the hidden Seyfert 1 nucleus, and hence could be the "mirror" envisaged by Antonucci & Miller. The aim of the observations presented here is to obtain a spectrum of the bright continuum peak through a small (0".3) aperture to isolate it from the surrounding narrow line nebulosity and enhance the chances of detecting a reflected broad-line component if it is present. Detection of broad emission lines in this spectrum would provide direct evidence for a hidden Seyfert 1 nucleus in NGC 1068.

In this *Letter* we address only the immediate aims of the observation. A detailed presentation of all the line fluxes and profiles, as well as results from our far-UV observations, will be presented in a future paper. In § 2 we discuss the observations, the data reduction procedure, and we present the spectra. Section 3 presents the results of line-profile fitting. Our conclusions are presented in § 4.

2. OBSERVATIONS, REDUCTION, AND SPECTRA

The observations were carried out on 1990 October 29, with the Faint Object Spectrograph (FOS) red detector using the G270H, G400H, and G570H gratings, yielding spectra in the ultraviolet, blue, and red, respectively. Each exposure was 300 s.

The observations began with a three-stage target acquisition sequence designed to center the continuum peak of NGC 1068 in the 0".3 aperture (see Kinney & Ford 1990 for a description of FOS target acquisition). We are confident that the final pointing of the telescope was centered on the continuum peak to within an accuracy of 0".1. The resulting FOS spectra were calibrated using recent observations obtained as part of the Science Verification (SV) phase of the mission. The flux scale was multiplied by a factor of 5 to take into account aperture losses from a point source. Wavelengths were calibrated using the internal Pt-Cr-Ne hollow cathode lamps. For the G570H grating, a wavelength comparison spectrum was obtained during these observations of NGC 1068. Wavelength calibration for the G270H and G400H spectra use previously

[1] Bloomberg Center for Astrophysics, Johns Hopkins University, Baltimore, MD 21218.
[2] Physics Department, University of California Santa Barbara, Santa Barbara, CA 93106.
[3] Space Telescope Science Institute, 3700 San Martin Drive, Baltimore, MD 21218.
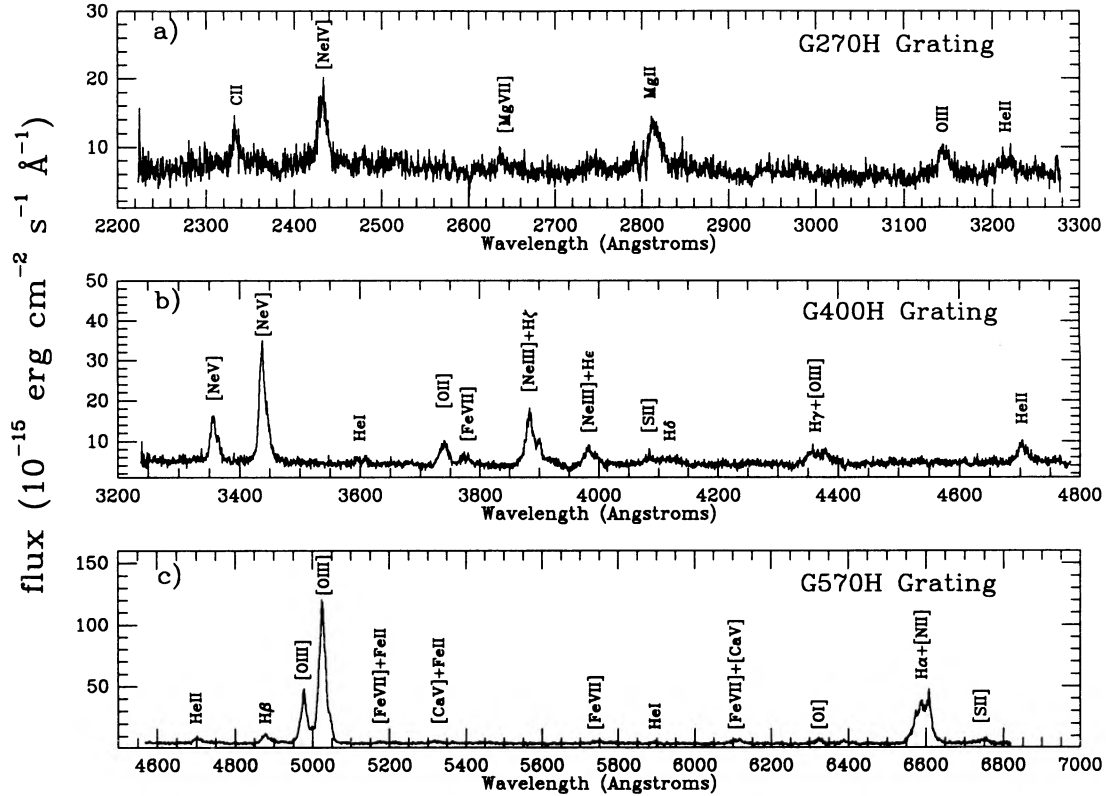[4] Code C-011 Cass, University of California San Diego, La Jolla, CA 92093.

FIG. 1.—Spectra of the nucleus of NGC 1068. (a) G270H grating spectrum from 2200 to 3300 Å; (b) G400H grating spectrum from 3200 to 4800 Å; (c) G570H grating spectrum from 4600 to 7000 Å. Flux-density scale is in units of 10^{-15} ergs cm^{-2} s^{-1} Å^{-1}.

obtained SV data. Overlapping regions of the G400H and G570H spectra indicate that the wavelength scales for these two spectra agree to within 0.15 Å. Included in the wavelength calibration is a correction for geomagnetically induced image motion (Junkkarinen et al. 1991) which affects the red detector. Our calibrated spectra are shown in Figure 1.

An important result from the G270H spectrum is that the UV continuum flux density is lower than the *IUE* continuum flux density by a factor of about 7, which implies that the source of the UV continuum is spatially extended. Far-UV observations which will be presented in a future paper support this.

3. LINE PROFILES

The spectrum is dominated by emission lines with integrated full width at half-maximum (FWHM) of around 1200 km s^{-1}, with many of the lines exhibiting a red wing. The line profiles are clearly more complex than Gaussian, suggesting that we observe more than one distinct velocity component in our aperture. We have employed a technique of line-profile fitting to determine accurate fluxes and to account for blending between neighboring emission lines.

There is very little reddening along our line of sight to NGC 1068. The ratio of the Helium Paschen lines He I $\lambda3204$/He I $\lambda4686 = 0.39$ suggests that the reddening is less than $E(B - V) = 0.12$ mag. This is supported by the lack of any 2200 Å feature (Bohlin & Savage 1981) in the *IUE* spectrum of NGC 1068 (and in our far-UV spectrum). From the ratio of [O II] $\lambda3729$/[O II] $\lambda3726 = 0.5 \pm 0.2$ we estimate the electron density to be on the order of 1200 cm^{-3}. The error on this

estimate is fairly large because the [O II] doublet is not well resolved. Unfortunately there is insufficient signal in the [S II] $\lambda6717, 6731$ doublet to yield an independent density estimate. The ratio of [O III] $\lambda\lambda4959, 5007$/[O III] $\lambda4363 = 49 \pm 8$ indicates an electron temperature of 18,000 K in the low-density limit. These estimates derived from narrow lines in our spectrum reflect the physical conditions in the narrow line clouds which illuminate our aperture—in particular clouds B and C in Paper I.

A central aim of these observations is to determine whether we detect a scattered broad-line component in the Hβ profile. To this end, we fitted the [O III] $\lambda\lambda4959, 5007$ and Hβ lines with a superposition of Gaussian functions. These Gaussian components are mathematical approximations to the profile which may not actually represent physical entities. Table 1 lists the results of the line fitting. The errors quoted in Table 1 are formal 90% confidence limits obtained from the covariance matrix of the fit using the method described by Lampton, Margon, & Bowyer (1976). These errors do not include systematic errors in the absolute flux calibration and the absolute wavelength calibration. The uncertainty in the absolute wavelength calibration could be 1 or 2 Å (~ 100 km s^{-1} at 5000 Å) and will not be fully known until further tests are carried out with *HST*. The integrated flux, peak wavelength, and integrated full width at half-maximum are also listed in Table 1. Relative errors for the line-component redshifts are typically about 100 km s^{-1}.

Examples of the profile fits are shown in Figure 2 where we present observed redshifts with respect to a systemic velocity of 1151 km s^{-1} (Rood 1982). The instrumental profile for these

TABLE 1

EMISSION-LINE PARAMETERS

Line ID (1)	cpt (2)	Flux ($\times 10^{15}$ ergs cm^{-2} s^{-1}) (3)	Redshift (km s^{-1}) (4)	FWHM (km s^{-1}) (5)
Hβ λ4861.........	1	70 ± 48	760	990 ± 600
	2	10 ± 9	1000	333 ± 1
	3	90 ± 33	1500	2200 ± 540
Integrated......	...	170 ± 38	980	1000 ± 190
[O III] λ5007......	1	1580 ± 59	950	1100 ± 24
	2	160 ± 61	1000	340 ± 100
	3	590 ± 45	1100	2340 ± 100
	4	60 ± 39	1500	260 ± 140
	5	140 ± 21	2300	630 ± 80
Integrated......	...	2540 ± 91	1080	1000 ± 25

NOTES.—Col. (1): Line identification; col. (2): Gaussian component number; col. (3): Flux in component with 90% confidence error; col. (4): Observed redshift of component; col. (5): FWHM of component with 90% confidence error.

observations has FWHM of approximately 230 km s^{-1}. We have not attempted to deconvolve the instrumental width from the values in Table 1. Figure 2a illustrates the Gaussian decomposition of [O III] $\lambda\lambda$4959, 5007 which provides a good fit with minimum reduced χ^2 of 1.26 with 203 degrees of freedom. Most of the flux (65%) is in a component with FWHM of 1150 km s^{-1}, and there is a red wing due to a component with FWHM of 630 km s^{-1} shifted some 1300 km s^{-1} redward of the main line. There is also a weak, but significant, broad component to [O III] $\lambda\lambda$4959, 5007 with FWHM of 2300 km s^{-1} which accounts for 20% of the total flux. This broad component has previously been observed in the nucleus of NGC 1068 by Pelat & Alloin (1980) and Alloin et al. (1983). Neither of these papers, however, find a component analogous to the extreme redshifted component seen in our FOS spectra.

Figure 2b illustrates the Gaussian decomposition of Hβ obtained from the simultaneous fitting of Hβ, Hα, and [N II] $\lambda\lambda$6548, 6584. This model is not as robust as that for [O III] $\lambda\lambda$4959, 5007 because of the heavy blending of Hα with [N II] $\lambda\lambda$6548, 6584, but the fit obtained is excellent, giving a

minimum value for the reduced χ^2 of 1.09 with 298 degrees of freedom. We use a three component fit to Hα and Hβ with two components for [N II] $\lambda\lambda$6548, 6584. The hydrogen lines exhibit analogous components to [O III] λ5007, a narrow component with FWHM of 300 km s^{-1}, a broader component of 1000 km s^{-1} FWHM, and a strong broad component of 2200 km s^{-1} FWHM which accounts for 50% of the total flux in Hβ. To avoid confusion, we hereafter refer to the broad polarized Hβ component observed by Antonucci & Miller (1985) as the "BLR component" which we argue below is distinct from the "broad" Hβ component with FWHM of 2200 km s^{-1}. In contrast with the [O III] λ5007 profile, the broad component in Hβ is redshifted with respect to the narrower component by 740 km s^{-1}. Antonucci and Miller find that the BLR component of Hβ observed in the polarized spectrum is redshifted with respect to the narrow component by 600 km s^{-1}. Gaussian fits to the higher order Balmer lines indicate that they also appear to be dominated by broad components with FWHM of $\sim$2200 km s^{-1}.

To clarify whether we detect the BLR Hβ component observed in polarized light, we model the FOS Hβ line profile as a combination of a narrow component and a BLR component with all parameters fixed except for the amplitudes. For the narrow component of Hβ we use the [O III] λ5007 line profile modeled as above by five Gaussian components (see Fig. 2a). The redshift and width of each component in this model is fixed at the value derived for [O III] λ5007, and only the amplitude of the integrated profile is allowed to vary. For the BLR component of Hβ, we use a single Gaussian redshifted with respect to the peak of the narrow component by 600 km s^{-1} and with a fixed FWHM of 3030 km s^{-1}. The fixed parameters for the BLR component are taken from the ground-based nuclear polarized flux profile (Miller et al. 1991). By calculating the variation of the minimum χ^2 as a function of the amplitude of the BLR component, we find that at the 90% confidence level we can only put an upper limit on the flux of the BLR component of approximately 80×10^{-15} ergs cm^{-2} s^{-1}. The minimum χ^2 value of the BLR component flux is $(30 \pm 40) \times 10^{-15}$ ergs cm^{-2} s^{-1} (see Fig. 2c). MGM estimate the total reflected BLR Hβ flux from the nucleus of NGC 1068 to be 320×10^{-15} ergs cm^{-2} s^{-1}. We certainly do not detect a
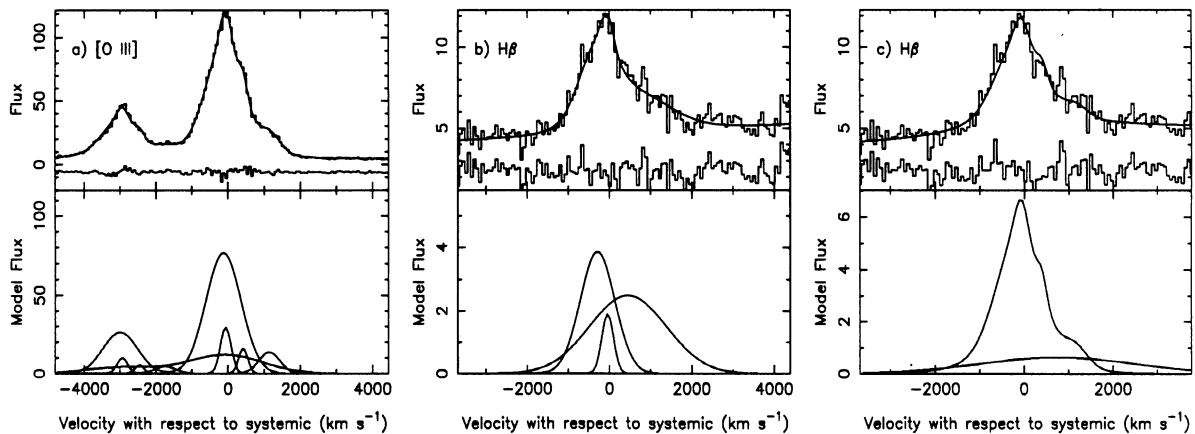

FIG. 2.—Line-profile models. Top half of each panel illustrates the spectrum overlayed with the model profile and the residual. Bottom half of each panel illustrates the different components used in the model. (a) Five Gaussian component model for [O III] $\lambda\lambda$4959, 5007; (b) three Gaussian component model of Hβ derived from simultaneously fitting Hβ, Hα, and [N II] $\lambda\lambda$6548, 6584. (c) Model for Hβ derived from a superposition of the rescaled [O III] $\lambda\lambda$4959, 5007 profile and a Gaussian component with FWHM of 3030 km s^{-1}.

component with this flux, and in fact it is larger than the total emission in our Hβ line. Thus we conclude that either the continuum peak is not the mirror, or the mirror must be extended with respect to our 0″3 aperture. The equivalent width represented by our upper limit on the BLR contribution is 16 Å. This is much less than the equivalent width of 300 Å for the BLR component in the polarized spectrum of MGM, suggesting that the FOS continuum is dominated by some source other than the reflected continuum. Alternatively, the equivalent width of the scattered BLR component with respect to the scattered continuum may not be constant over the reflection region. Since we do not detect the BLR component in Hβ, we must also conclude that the [O III] λ5007 line profile and the Hβ profile are not significantly different at the 90% confidence level.

It is important to consider the effects of the large *HST* point spread function (PSF) (Burrows et al. 1991) on our ability to detect any BLR component. If the mirror is a point source, only 20% of the flux from the mirror is admitted by the 0″3 aperture, while the flux density from an extended background (e.g., stars and narrow line clouds) is less attenuated. Thus the large PSF decreases the BLR equivalent width by a factor of 5 (or less depending on the spatial extent of the mirror and the background) from what is expected with an ideal *HST* PSF. We are still, however, an order of magnitude better than a ground-based observation using a 2″ aperture. The technique we use to determine the upper limit on the BLR flux in our spectrum already takes into account the loss of sensitivity contributed by the extended continuum. Thus our conclusions hold, regardless of the effect that the PSF has on our sensitivity.

MGM model the electron scattering plasma as a hot ($T \sim 3 \times 10^5$ K) cone which begins $\sim$30 pc (or $\frac{1}{2}$″) from the hidden nucleus and extends to $\sim$300 pc (5″). This interpretation is supported by our suggestion that the UV continuum is extended, and is consistent with the nondetection of a BLR component in our spectrum. But we note that if MGM's size is correct, the [O III] images in Paper I show that there are cool, high-density clouds embedded in the hot plasma. If the [O III] clouds have densities ($\sim 10^3$ cm^{-3}), as derived above, they cannot be stable and be as close to the nucleus as the hot plasma. If they were, the clouds would rapidly become so highly ionized that we would not observe ions like O^{++}. To increase their lifetime the clouds would have to be denser than our measurements suggest.

4. CONCLUSIONS

The spectrum we observe is dominated by lines with integrated FWHM of around 1200 km s^{-1}. The lines generally exhibit a red wing, and the complex shape of their profiles is evidence that we observe at least several different velocity components within the aperture. Both the Balmer lines and the strong forbidden lines show evidence for a broad component with FWHM on the order of 2200 km s^{-1}.

A broad component with FWHM of 2200 km s^{-1} provides 50% of the total flux in Hβ. However, this component is narrower than the BLR component observed in polarized light. An error analysis shows that we do not detect the BLR component with FWHM of 3030 km s^{-1}. Thus we conclude that the continuum peak is not the mirror, or that the reflection region is extended with respect to our 0″3 aperture. In the latter case, the equivalent width of the Hβ BLR line, if present at all, is much weaker than expected from the nuclear polarized-flux spectrum presented by MGM.

REFERENCES

Alloin, D., Pelat, D., Boksenberg, A., & Sargent, W. L. W. 1983, ApJ, 275, 493
Antonucci, R. R., & Miller, J. S. 1985, ApJ, 297, 621
Bohlin, R. C., & Savage, B. D. 1981, ApJ, 249, 109
Burrows, C. J., Holtzman, J. A., Faber, S. M., Bely, P. Y., Hasan, H., Lynds, C. R., & Schroeder, D. 1991, ApJ, 369, L21
Evans, I. N., Ford, H. C., Kinney, A. L., Antonucci, R. R. J., Armus, L., & Caganoff, S. 1991, ApJ, 369, L27 (Paper I)
Junkkarinen, V. T., Beaver, E. A., Cohen, R. D., Hier, R., Lyons, R., & Rosenblatt, E. 1991, BAAS, 22, 1283
Kinney, A. L., & Ford, H. C. 1990, FOS Target Acquisition Handbook, Version 2.1 (Baltimore: STScI)

Lampton, M., Margon, B., & Bowyer, S. 1976, ApJ, 208, 177
Lynds, C. R., et al. 1991, ApJ, 369, L31
Miller, J. S., Goodrich, R. W., & Mathews, W. G. 1991, ApJ, in press
Osterbrock, D. E. 1989, Astrophysics of Gaseous Nebulae and Active Galactic Nuclei (Mill Valley: University Science Books)
Pelat, D., & Alloin, D. 1980, A&A, 81, 172
Planesas, P., Scoville, N., & Myers, S. T. 1991, ApJ, 369, 364
Pogge, R. W. ApJ, 328, 519
Rood, H. 1982, ApJS, 49, 111